Junctional-fluctuation-mediated fluidization of multi-phase-field epithelial monolayers

James N. Graham [1] and Jan Rozman [1,2,3,*]

[1] *Rudolf Peierls Centre for Theoretical Physics, University of Oxford, Oxford OX1 3PU, United Kingdom*

[2] *Jožef Stefan Institute, Jamova 39, SI-1000 Ljubljana, Slovenia*

[3] *University of Ljubljana, Faculty of Mathematics and Physics, Jadranska 19, SI-1000 Ljubljana, Slovenia*

(Received 27 August 2025; accepted 30 July 2026; published 24 August 2026)

We analyze a multi-phase-field model for an epithelial monolayer with pairwise adhesions between neighboring cells following an Ornstein-Uhlenbeck process, representing the stochastic turnover of junctional molecular motors. These fluctuations in junctional adhesion result in rearrangements in the tissue, fluidizing it and producing diffusive cell motion. Similar junctional fluctuations have proven a very useful tool in the vertex model literature, and we hope they will be equally helpful to the multi-phase-field model approach. Moreover, we observe that the cells' effective diffusion coefficient depends nonmonotonically on the persistence time of the fluctuations, confirming results previously observed in the vertex model.

DOI: 10.1103/lbph-g5kd

I. INTRODUCTION

The physics of epithelial cells and tissues, their rearrangements, and their motion has been of long interest [1–3]. Epithelia have been studied using a range of theoretical and computational approaches such as continuum models [4–6], particle-based models [7–9], and cellular Potts models [10–12].

One extensively used approach to modeling epithelial monolayers are 2D vertex models [13–17]. In this formalism, cells are represented as polygons tiling the surface, with their vertices moving in response to forces. One avenue of research in vertex models has been understanding the role of junctional tension fluctuations, as would arise from the stochastic turnover of junctional molecular motors, in the rearrangement and motion of cells. This was modeled by the junctional tensions in the vertex model following an Ornstein-Uhlenbeck process [18–21]: such tension fluctuations can induce T1 transitions, thereby fluidizing the tissue. Notably, Ref. [21] reported that the effective diffusion coefficient of cells in the resulting fluidized tissue depends nonmonotonically on the persistence time of the tensions.

Fluctuating tensions in the vertex model formalism have proven a very useful tool and have been used in studies of, e.g., wound healing [22], cell sorting [19], budding in three dimensions [23,24], nematic forces with a global direction [25], and long-range order in tissues [26]. Multi-phase-field models [1,27–31] are another approach to modeling tissues, representing each cell as a field. While computationally more expensive than vertex models, they have several advantages in comparison to them: (i) they allow for a more detailed description of cell shape and are not limited to polygons, (ii) they naturally capture T1 transitions without the need for a separate implementation, and (iii) they are not confined to confluent tilings, allowing for gaps and holes [32,33]. These advantages could prove helpful in contexts where the fluctuating-tensions vertex model had previously been used (e.g., spontaneous hole closure for modeling wound healing). Therefore, in this paper, we show and analyze an implementation of the junctional fluctuations approach into the multi-phase-field model formalism.

We introduce junctional fluctuations by modifying the cell-cell adhesion term in the model, with pairwise adhesions now following an Ornstein-Uhlenbeck process as has been done in vertex models. We show that, for appropriate values of the adhesion fluctuation variance and persistence, these fluctuations can indeed induce rearrangements and fluidize the multi-phase-field model. Interestingly, we also find a nonmonotonic dependence of the cells' effective diffusion coefficient, as has previously been observed in the vertex model [21].

II. PHASE-FIELD MODEL

In the multi-phase-field model, each cell i is represented by a phase field $\varphi^{(i)}(\mathbf{x},t)$ [29], which takes value 1 inside and 0 outside the cell. The dynamics of the phase fields are given by the equation of motion

$$\partial_t \varphi^{(i)} + \mathbf{v}^{(i)} \cdot \nabla \varphi^{(i)} = -J_0 \frac{\delta \mathcal{F}}{\delta \varphi^{(i)}}, \tag{1}$$

where $\mathbf{v}^{(i)}(\mathbf{x},t)$ is the velocity of the phase field $\varphi^{(i)}(\mathbf{x},t)$, $\mathcal{F}$ is the free energy of the tissue, and the right hand side represents the relaxation to a free energy minimum at a rate J_0. The velocity $\mathbf{v}^{(i)}(\mathbf{x},t)$ is determined in the overdamped regime by the local force density acting on the cell,

$$\xi \mathbf{v}^{(i)}(\mathbf{x},t) = \mathbf{f}^{(i)}(\mathbf{x},t), \tag{2}$$

*Contact author: jan.rozman@ijs.si

where ξ is a friction coefficient and the force density is

$$\mathbf{f}^{(i)}(\mathbf{x},t) = \frac{\delta \mathcal{F}}{\delta \varphi^{(i)}} \nabla \varphi^{(i)}. \tag{3}$$

The free energy $\mathcal{F} = \mathcal{F}_{\mathrm{CH}} + \mathcal{F}_{\mathrm{area}} + \mathcal{F}_{\mathrm{rep}} + \mathcal{F}_{\mathrm{adh}}$ has four contributions [29,34,35]:

$$\mathcal{F}_{\mathrm{CH}} = \sum_i \frac{\gamma}{\lambda} \int d\mathbf{x} [(\varphi^{(i)})^2 (1-\varphi^{(i)})^2 + \lambda^2 (\nabla \varphi^{(i)})^2], \tag{4a}$$

$$\mathcal{F}_{\mathrm{area}} = \sum_i \mu \left[1 - \frac{1}{\pi R^2} \int d\mathbf{x}\, (\varphi^{(i)})^2 \right]^2, \tag{4b}$$

$$\mathcal{F}_{\mathrm{rep}} = \sum_i \sum_{j \neq i} \frac{\kappa}{\lambda} \int d\mathbf{x}\, (\varphi^{(i)})^2 (\varphi^{(j)})^2, \tag{4c}$$

$$\mathcal{F}_{\mathrm{adh}} = \sum_i \sum_{j \in \mathcal{N}_i(t)} \omega_{ij} \lambda \int d\mathbf{x}\, \nabla [(\varphi^{(i)})^2] \cdot \nabla [(\varphi^{(j)})^2]. \tag{4d}$$

Of these, the first is a Cahn-Hilliard term favoring phase separation into regions of $\varphi^{(i)} = 0$ or 1. This results in an interface of width $\mathcal{O}(\lambda)$ lattice units, interpreted as the cell membrane, with γ/λ being an energy scale. The second term is a soft area constraint with strength μ and equilibrium cell area πR^2 given by the radius R. The third term imposes a penalty on cell-cell overlap with an energy scale κ/λ.

The fourth term in the free energy describes the adhesion of cell membranes by computing the dot product of the gradients of the squares of each pair of phase fields. The inside (outside) of a cell corresponds to $\varphi = 1$ ($\varphi = 0$) so when two phase-field cells are next to each other, the gradients of their squares point in approximately opposite directions. The strength of the adhesion between cells i and j is given by ω_{ij}, and it is energetically favorable (unfavorable) for the interfaces of cells i and j to overlap when ω_{ij} is positive (negative). The total adhesive free energy is computed as a pairwise sum over all neighbors, where $\mathcal{N}_i(t)$ denotes the set of neighbors of cell i at time t. Two cells i and j are said to be neighbors when their phase fields $\varphi^{(i)}$ and $\varphi^{(j)}$ both take values greater than 0.2 on the same lattice site. This adhesive term broadly corresponds to the line tension term in vertex models [14,19], which captures both tension and cell-cell adhesion.

This adhesion free energy functional, which matches that of Chiang *et al.* [36] and is similar to that of Nonomura [27], differs from those of some previous works [34,37] in two key ways. First, in this formulation, the functional derivative of $\mathcal{F}_{\mathrm{adh}}$ that appears on the right-hand side of Eq. (1) is proportional to $\varphi^{(i)}$. A previous implementation of adhesion in the multi-phase-field model [34] does not have this proportionality. In developing the model presented here, we found that this can in general lead to numerical instability when ω is large (see Sec. I in the Supplemental Material [38]). Second, other works have considered a single energy scale ω for all adhesive interactions, while here we implement a set of pairwise $\{\omega_{ij}\}$ so that each pair of cells can have its own adhesion strength.

These ω_{ij} are the avenue through which we introduce junctional fluctuations to the model, representing the stochastic turnover of junctional molecular motors. We demand symmetry in the energy scales, $\omega_{ij} = \omega_{ji}$. The values of ω_{ij} follow an Ornstein-Uhlenbeck process, as had previously been done in vertex models [18,19,21,25]:

$$\frac{d\omega_{ij}(t)}{dt} = -\frac{1}{\tau_\omega} \omega_{ij}(t) + \xi_{ij}(t), \tag{5}$$

where ξ_{ij} is Gaussian white noise with properties $\langle \xi_{ij}(t) \rangle = 0$ and $\langle \xi_{ij}(t) \xi_{kl}(t') \rangle = (2\sigma_\omega^2/\tau_\omega)\delta_{ik}\delta_{jl}\delta(t-t')$; τ_ω is the persistence time and σ_ω^2 is the long-time variance of the adhesion fluctuations. Because the strength of adhesion is only meaningful between adjacent cells, $\omega_{ij}(t)$ is only evolved with time if cells i, j are neighbors [determined in the same way as described for Eq. (4d)]; otherwise, it is set to 0. This means that when a pair of cells newly come into contacts their adhesion is zero.

We simulate 100 cells in a rectangular domain with side lengths $L_x = 150$ and $L_y = 130$ lattice units and periodic boundary conditions. The cells are initialized in a regular hexagonal geometry. We allow the system to run for 3×10^4 time units before taking measurements. Time $t = 0$ corresponds to the start of measurements, and the simulation then runs until time $t = T = 1.8 \times 10^5$. Data about the state of the tissue is output in intervals of length $\delta t = 1000$.

The parameters assigned to the free energy terms in Eq. (4) are $\gamma = 1.4$, $\lambda = 2.0$, $\mu = 120$, and $\kappa = 1.5$. The coefficient of friction in Eq. (2) is $\xi = 3.0$ and the target cell area is given by radius $R = 8.0$ (in lattice units). Relaxation according to Eq. (1) is controlled by the rate $J_0 = 10^{-2}$. The phase-field Eqs. (1)–(4) are solved using a one-step predictor-corrector method. The unit of time is 1, and each unit is divided into five timesteps. The method of solving the phase-field model is outlined further in [29,35]. The adhesion fluctuations of Eq. (5) are solved using a finite difference method on each timestep.

III. RESULTS

An epithelial monolayer can change its topology through several processes, such as cell divisions and extrusions [6,39–41]. Fluidization of a tissue through fluctuating tensions/adhesions at cell-cell junctions relies on cell intercalations (i.e., T1 transitions) that are able to modify neighbor-neighbor contacts [20,39,42]. During a T1 transition, the junction between one pair of cells shrinks and a new junction forms between another previously unconnected pair of cells. Each of the two cells that were neighbors before the transition loses one neighbor, while each of the two cells that are neighbors after the transition gains one.

We first show that a T1 can be induced in the multi-phase-field model by modulating the pairwise cell adhesions ω_{ij} (Fig. 1 and Movie S1). In Fig. 1(a), the cells outlined in red are stuck together by a large positive $\omega_{ij} = +10$, whereas all other pairwise adhesions are given by $\omega_{ij} = 0.4$. In this simulation, the adhesions do not fluctuate (i.e., $\sigma_\omega = 0$). However, we switch the adhesion parameter for the red cells abruptly to -10, resulting in the cells being pushed apart as shown in Fig. 1(b). The cells transition through the equivalent of a fourfold vertex until the cell intercalation is completed in Fig. 1(c). So that the system does not arrest before completing the T1, we add a noise term $D_\varphi \eta$ to the RHS of Eq. (1) for this simulation, where η is unit-variance Gaussian noise and $D_\varphi = 0.1$.

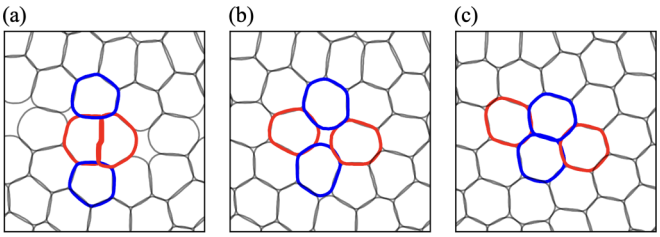

FIG. 1. A quartet of cells (a) before, (b) during, and (c) after a T1 topological transition in an adhesive background. The red cells at first attract with $\omega_{ij} > 0$ (a) and then repel with $\omega_{ij} < 0$ (b), while the blue cells attract with $\omega_{ij} > 0$ to complete the transition (c).

We next turn to simulating a tissue with all pairwise adhesions fluctuating following Eq. (5) [without the additional $D_\varphi \eta$ term in Eq. (1)]. We first set $\sigma_\omega = 0.1$ and $\tau_\omega = 10^3$. The resulting monolayer is shown in Fig. 2(a) and Movie S2: the system, despite fluctuations in ω_{ij}, is solidlike (i.e., cells do not exchange neighbors) and remains in a regular hexagonal lattice.

Keeping $\tau_\omega = 10^3$, we next perform a simulation at a higher $\sigma_\omega = 1.1$, with the resulting model tissue shown in Fig. 2(b) and Movie S3. The larger fluctuations in adhesion resulting from a higher σ_ω can now overcome the energy barriers associated with neighbor exchanges, enabling cells to escape from their local neighborhood through a series of T1 transitions and become mobile, producing a disordered, fluidlike tissue.

To quantify the difference in mobility between the two cases, we measure the mean-square displacement

$$\mathrm{MSD}(t) = \frac{1}{N}\sum_{i=1}^{N} |\mathbf{r}^{(i)}(t) - \mathbf{r}^{(i)}(0)|^2, \tag{6}$$

where N is the number of cells and $\mathbf{r}^{(i)}$ is the center-of-mass position of cell i at time t. As expected, in the solidlike model tissue, MSD saturates at a small value (less than the cell radius R), as shown in Fig. 2(a). In a fluidized layer, however, the MSD grows linearly in time [Fig. 2(b)].

As a second measure of fluidization, we also estimate how often cells gain and lose neighbors. Specifically, we compare how the set of neighbors $\mathcal{N}_i(t)$ of cell i changes between subsequent outputs of the tissue state, which are separated in time by $\delta t = 1000$. For each neighboring cell that is either added or removed from $\mathcal{N}_i(t)$, the number of the cell's neighbor change events ΔN_i is incremented by 1; as the tissue states are only compared every δt, this does not account for every change of the neighbor structure, but allows for a comparison of such events between different simulations. Note that a cell can separate and reconnect with another cell multiple times while remaining in the same general neighborhood.

The resulting plots of ΔN_i averaged over all cells are shown in Figs. 2(e) and 2(f). There are no neighbor changes in the solidlike tissue [Fig. 2(e)] but the average number of changes grows linearly in the fluidlike tissue [Fig. 2(f)], revealing a constant rate of neighbor exchange. The presence of neighbor changes, in conjunction with the diffusive MSD, discounts solid flocking [34] as the origin of the measured cell mobility.

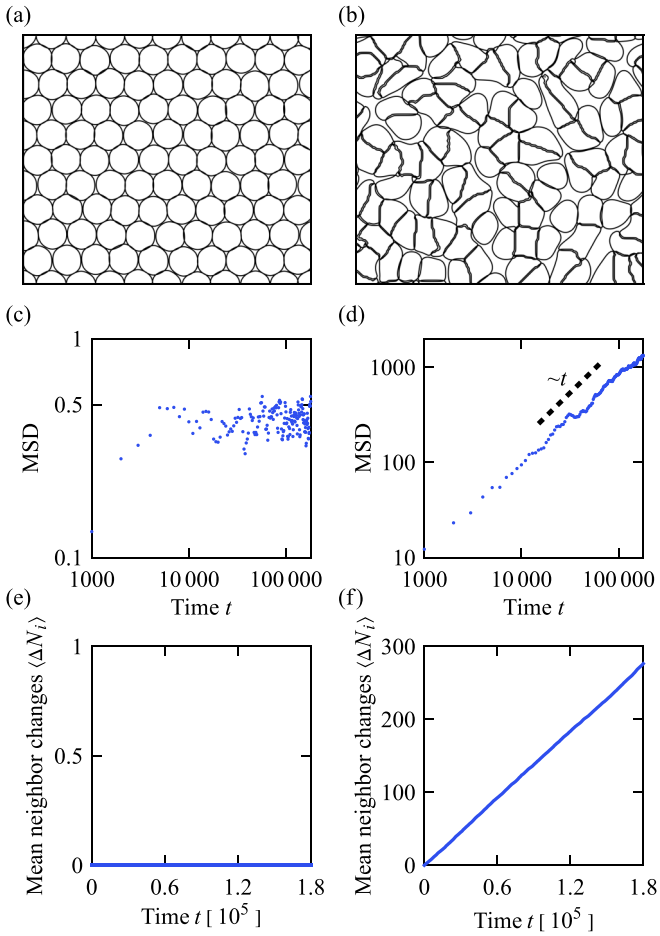

FIG. 2. (a), (b) Model tissue with (a) $\sigma_\omega = 0.1$, $\tau_\omega = 10^3$ and (b) $\sigma_\omega = 1.1$, $\tau_\omega = 10^3$. The larger σ_ω in (b) permits greater variance in ω_{ij}, which result in intercalations and diffusive behavior. Note that the long contacts of some cell pairs arise from high adhesion between those cells; the jagged cell interfaces in the regime of high adhesion fluctuations are an artifact arising from the lattice underpinning the multi-phase-field simulations. (c), (d) Mean-square displacement plotted against time for the systems in (a) and (b), respectively. (e), (f) Average neighbor changes plotted against time for the systems in (a) and (b), respectively. The solid phase exhibits no neighbor changes whereas the fluid phase has a constant rate of neighbor turnover.

We then perform a scan of $\tau_\omega - \sigma_\omega$ parameter space and characterize the resulting monolayers using the effective diffusion coefficient, the average number of a cell's neighbor-change events, and the hexatic order parameter. These quantities are illustrated in heatmaps in Fig. 3. The effective diffusion coefficient is calculated as $D_{\mathrm{diff}} \equiv \mathrm{MSD}(T)/(4T)$, where $T = 1.8 \times 10^5$ is the final simulation time. At a given τ_ω, the effective diffusion coefficient D_{diff} increases with σ_ω. However, we find that D_{diff} depends nonmonotonically on τ_ω [Fig. 3(a)]. This is in agreement with the observations of Yamamoto *et al.* in the vertex model [21].

We then plot how the final value at $t = T$ of estimated neighbor change events averaged over all cells $\langle \Delta N_i \rangle$ depends on σ_ω and τ_ω in Fig. 3(b). A solid phase should exhibit no neighbor rearrangements (except possibly initially as the

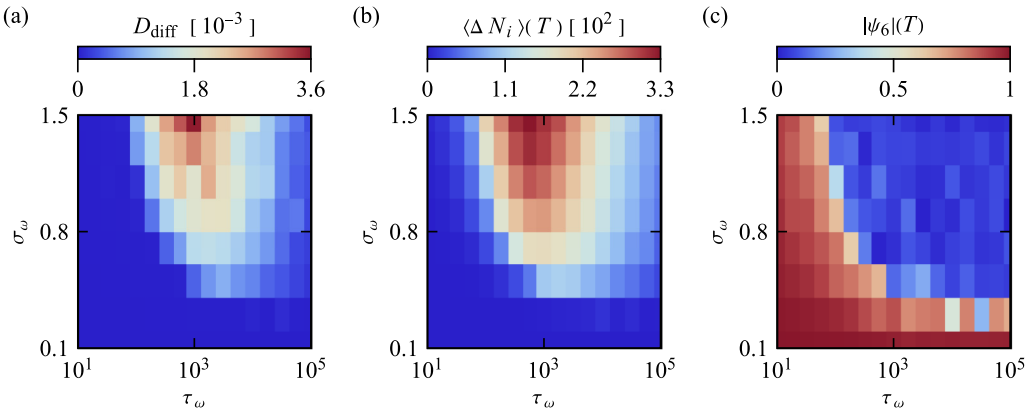

FIG. 3. Heatmaps of (a) the effective diffusion coefficient D_{diff}, (b) the final average estimated number of neighbor change events $\langle \Delta N_i \rangle$, and (c) final $|\psi_6|$ in $\tau_\omega - \sigma_\omega$ phase space. Panels (a) and (b) show that the effective diffusion coefficient and the number of neighbor change events depend nonmonotonically on τ_ω. Panel (c) illustrates the change from high to low $|\psi_6|$, indicating, respectively, a regular hexagonal lattice and a disordered state.

model tissue relaxes), whereas cells in a fluid phase should change neighbors regularly. Indeed, we observe that for sufficiently large τ_ω and σ_ω, neighbor changes occur at a finite rate. Just as for the effective diffusion coefficient, the dependence on τ_ω is nonmonotonic, so that there is an optimal τ_ω that maximizes the number of neighbor change events.

Finally, the hexatic order of the model tissue is quantified using the hexatic order parameter ψ_6, famously a feature of the KTHNY theory of crystal melting in two dimensions [43,44], that has previously been used to characterize structure in model tissues [26,40,45,46]. It is calculated as

$$\psi_{6j} = \frac{1}{N_j} \sum_{k \in \mathcal{N}_j} \exp(6i\theta_{k,j}), \tag{7}$$

where j, k index cells, $\mathcal{N}_j$ is the set of neighbors of cell j, N_j is the size of said set, and $\theta_{k,j}$ gives the angle of the center of mass of cell k with respect to that of cell j. We measure $|\psi_6| \equiv |\langle \psi_{6j} \rangle|$, the magnitude of the hexatic structure across all cells in a layer. As the initial condition is a regular hexagonal lattice, $|\psi_6|$ should take a value close to 1 for a solidlike state and close to 0 for a fluidlike state. A heatmap of final $|\psi_6|$ is shown in Fig. 3(c). As expected, the mean hexatic order parameter changes from around 1 to around 0 as τ_ω and σ_ω become sufficiently large, indicative of a transition from a regular hexagonal lattice to a disordered state.

The simulations are relatively computationally expensive, so that the final simulation time is comparable with the highest values of τ_ω we consider. However, the nonmonotonic behavior of D_{diff} and final $\langle \Delta N_i \rangle$ can already be observed for $\tau_\omega < 10^4$, so at least an order of magnitude smaller than the simulation time (Fig. S1 [38]). Moreover, at $\tau_\omega = 10^4$ and even $\tau_\omega = 10^5$, the MSD plots are still approximately diffusive on the simulation timescale (Fig. S2 [38]); the final MSD at $\tau_\omega = 10^4$ and $\sigma_\omega = 1.5$ also corresponds to cell displacement by more than two cell diameters. Together, these suggest that the nonmonotonic dependence on τ_ω is a property of the system and not a consequence of the simulation length.

In addition, the diffusive nature of the MSD at high τ_ω discounts that the nonmonotonic dependence arises from a transition to a solid flock. Moreover, while the number of neighbor changes decreases with increasing τ_ω in this part of the parameter space, neighbor changes do still happen [Figs. 3(b) and S3 [38]]. Both the absence of a solid flock and the presence of neighbor changes can be seen in Movies S4 and S5, which show the evolution of the tissue at $\sigma_\omega = 1.1$ with $\tau_\omega = 10^4$ and $\tau_\omega = 10^5$, respectively.

We also remark that in our model, adhesion between newly neighboring cell pairs is set to 0 as discussed above. However, Yamamoto *et al.* [21] found that the nonmonotonic behavior in the vertex model remained for different rules of how tension was determined following a T1 transition. Therefore, it can be hoped that our choice of adhesion value for new neighbors also does not notably affect the qualitative results in the multi-phase-field model. Lastly, in Sec. II of the Supplemental Material [38], we show that the model can give cell velocity estimates that are broadly comparable with experimental values.

IV. DISCUSSION

We studied a multi-phase-field model for an epithelium [29,34] augmented with fluctuating pairwise adhesions following an Ornstein-Uhlenbeck process, representing the stochastic turnover of junctional motors. We showed that adhesion fluctuations result in rearrangements leading to diffusive motion of cells in the model monolayer. This provides another fluidization mechanism for phase-field models, focusing on the role of cell-cell junctions, rather than cell-scale polar [34,47] or nematic [29,37] activity.

Such Ornstein-Uhlenbeck fluctuations have previously been studied as a fluidization mechanism in vertex models [18–21]. Our work validates these results for a different type of discrete cell-level model. Moreover, we find the cells' effective diffusion coefficient to have a nonmonotonic dependence on persistence time in adhesion fluctuation, in agreement with what was reported in the vertex model [21]. That study suggested the nonmonotonic dependence arises from a separation of timescales at large fluctuation persistence times, with the system reaching a nearly force balanced state quickly after a rearrangement and that state then becoming unstable again on the timescale of fluctuation persistence.

Given the considerable range of uses the fluctuating-tensions approach found in the vertex model literature, we hope that the model proposed here will also be a powerful tool for further studies using multi-phase-field models. In future work, pairwise adhesion terms could be modified to, e.g., also account for the length of cell-cell interfaces [48,49], respond to local tensions [42], or depend on cell shape [50].

ACKNOWLEDGMENTS

We wish to thank Ioannis Hadjifrangiskou, Matej Krajnc, Diogo E. P. Pinto, Gianmarco Spera, and Julia M. Yeomans for helpful discussion. We also wish to thank Matej Krajnc and Julia M. Yeomans for a careful reading of the manuscript. J.N.G. acknowledges Pembroke College, Oxford. J.R. acknowledges support from the UK Engineering and Physical Sciences Research Council (Award No. EP/W023849/1), the ERC Advanced Grant ActBio (funded as UKRI Frontier Research Grant No. EP/Y033981/1), and the Slovenian Research and Innovation Agency (research Project No. J1-70062, development funding pillar RSF-0106, and research core funding P1-0055).

DATA AVAILABILITY

The processed simulation data that support the findings of this article are publicly available [51]. The simulation code used is publicly available [52]. The code is based on Celadro by Romain Mueller.

[1] R. Alert and X. Trepat, Physical models of collective cell migration, Annu. Rev. Condens. Matter Phys. **11**, 77 (2020).
[2] W. Xi, T. B. Saw, D. Delacour, C. T. Lim, and B. Ladoux, Material approaches to active tissue mechanics, Nat. Rev. Mater. **4**, 23 (2019).
[3] S. Shankar, A. Souslov, M. J. Bowick, M. C. Marchetti, and V. Vitelli, Topological active matter, Nat. Rev. Phys. **4**, 380 (2022).
[4] J. Ranft, M. Basan, J. Elgeti, J.-F. Joanny, J. Prost, and F. Jülicher, Fluidization of tissues by cell division and apoptosis, Proc. Natl. Acad. Sci. USA **107**, 20863 (2010).
[5] X. Serra-Picamal, V. Conte, R. Vincent, E. Anon, D. T. Tambe, E. Bazellieres, J. P. Butler, J. J. Fredberg, and X. Trepat, Mechanical waves during tissue expansion, Nat. Phys. **8**, 628 (2012).
[6] T. B. Saw, A. Doostmohammadi, V. Nier, L. Kocgozlu, S. Thampi, Y. Toyama, P. Marcq, C. T. Lim, J. M. Yeomans, and B. Ladoux, Topological defects in epithelia govern cell death and extrusion, Nature (London) **544**, 212 (2017).
[7] B. Szabó, G. J. Szöllösi, B. Gönci, Zs. Jurányi, D. Selmeczi, and T. Vicsek, Phase transition in the collective migration of tissue cells: Experiment and model, Phys. Rev. E **74**, 061908 (2006).
[8] N. Sepúlveda, L. Petitjean, O. Cochet, E. Grasland-Mongrain, P. Silberzan, and V. Hakim, Collective cell motion in an epithelial sheet can be quantitatively described by a stochastic interacting particle model, PLoS Comput. Biol. **9**, e1002944 (2013).
[9] S. Garcia, E. Hannezo, J. Elgeti, J.-F. Joanny, P. Silberzan, and N. S. Gov, Physics of active jamming during collective cellular motion in a monolayer, Proc. Natl. Acad. Sci. USA **112**, 15314 (2015).
[10] F. Graner and J. A. Glazier, Simulation of biological cell sorting using a two-dimensional extended Potts model, Phys. Rev. Lett. **69**, 2013 (1992).
[11] J. A. Glazier and F. Graner, Simulation of the differential adhesion driven rearrangement of biological cells, Phys. Rev. E **47**, 2128 (1993).
[12] T. Hirashima, E. G. Rens, and R. M. H. Merks, Cellular Potts modeling of complex multicellular behaviors in tissue morphogenesis, Dev. Growth Differ **59**, 329 (2017).
[13] H. Honda and G. Eguchi, How much does the cell boundary contract in a monolayered cell sheet? J. Theor. Biol. **84**, 575 (1980).
[14] R. Farhadifar, J.-C. Röper, B. Aigouy, S. Eaton, and F. Jülicher, The influence of cell mechanics, cell-cell interactions, and proliferation on epithelial packing, Curr. Biol. **17**, 2095 (2007).
[15] A. G. Fletcher, M. Osterfield, R. E. Baker, and S. Y. Shvartsman, Vertex models of epithelial morphogenesis, Biophys. J. **106**, 2291 (2014).
[16] D. Bi, J. H. Lopez, J. M. Schwarz, and M. L. Manning, A density-independent rigidity transition in biological tissues, Nat. Phys. **11**, 1074 (2015).
[17] S. Alt, P. Ganguly, and G. Salbreux, Vertex models: From cell mechanics to tissue morphogenesis, Phil. Trans. R. Soc. B **372**, 20150520 (2017).
[18] S. Curran, C. Strandkvist, J. Bathmann, M. de Gennes, A. Kabla, G. Salbreux, and B. Baum, Myosin II controls junction fluctuations to guide epithelial tissue ordering, Dev. Cell **43**, 480 (2017).
[19] M. Krajnc, Solid–fluid transition and cell sorting in epithelia with junctional tension fluctuations, Soft Matter **16**, 3209 (2020).
[20] C. Duclut, J. Paijmans, M. M. Inamdar, C. D. Modes, and F. Jülicher, Nonlinear rheology of cellular networks, Cells Dev. **168**, 203746 (2021).
[21] T. Yamamoto, D. M. Sussman, T. Shibata, and M. L. Manning, Non-monotonic fluidization generated by fluctuating edge tensions in confluent tissues, Soft Matter **18**, 2168 (2022).
[22] R. J. Tetley, M. F. Staddon, D. Heller, A. Hoppe, S. Banerjee, and Y. Mao, Tissue fluidity promotes epithelial wound healing, Nat. Phys. **15**, 1195 (2019).
[23] J. Rozman, M. Krajnc, and P. Ziherl, Collective cell mechanics of epithelial shells with organoid-like morphologies, Nat. Commun. **11**, 3805 (2020).
[24] J. Rozman, M. Krajnc, and P. Ziherl, Morphologies of compressed active epithelial monolayers, Eur. Phys. J. E **44**, 99 (2021).
[25] C. Duclut, J. Paijmans, M. M. Inamdar, C. D. Modes, and F. Jülicher, Active T1 transitions in cellular networks, Eur. Phys. J. E **45**, 29 (2022).
[26] Y.-E. Keta and S. Henkes, Long-range order in two-dimensional systems with fluctuating active stresses, Soft Matter **21**, 5710 (2025).

[27] M. Nonomura, Study on multicellular systems using a phase field model, PLoS ONE **7**, e33501 (2012).
[28] S. Najem and M. Grant, Phase-field model for collective cell migration, Phys. Rev. E **93**, 052405 (2016).
[29] R. Mueller, J. M. Yeomans, and A. Doostmohammadi, Emergence of active nematic behavior in monolayers of isotropic cells, Phys. Rev. Lett. **122**, 048004 (2019).
[30] A. Moure and H. Gomez, Phase-field modeling of individual and collective cell migration, Arch. Comput. Methods Eng. **28**, 311 (2021).
[31] B. A. Camley and W.-J. Rappel, Physical models of collective cell motility: From cell to tissue, J. Phys. D: Appl. Phys. **50**, 113002 (2017).
[32] A. Ardaševa, R. Mueller, and A. Doostmohammadi, Bridging microscopic cell dynamics to nematohydrodynamics of cell monolayers, Soft Matter **18**, 4737 (2022).
[33] D. E. Pinto, J. Rozman, and J. M. Yeomans, Multi-phase field model reveals internal dissipation is crucial for spontaneous hole formation in cell monolayers Nat. Commun. **17**, 8288 (2026).
[34] G. Zhang, R. Mueller, A. Doostmohammadi, and J. M. Yeomans, Active inter-cellular forces in collective cell motility, J. R. Soc. Interface **17**, 20200312 (2020).
[35] R. Mueller and A. Doostmohammadi, Phase field models of active matter, arXiv:2102.05557.
[36] M. Chiang, A. Hopkins, B. Loewe, D. Marenduzzo, and M. C. Marchetti, Multiphase field model of cells on a substrate: From three dimensional to two dimensional, Phys. Rev. E **110**, 044403 (2024).
[37] G. Zhang and J. M. Yeomans, Active forces in confluent cell monolayers, Phys. Rev. Lett. **130**, 038202 (2023).
[38] See Supplemental Material at http://link.aps.org/supplemental/10.1103/lbph-g5kd for additional model discussion, Figs. S1–S3, and captions for Movies S1–S5.
[39] M. Merkel, R. Etournay, M. Popović, G. Salbreux, S. Eaton, and F. Jülicher, Triangles bridge the scales: Quantifying cellular contributions to tissue deformation, Phys. Rev. E **95**, 032401 (2017).
[40] S.-Z. Lin, M. Merkel, and J.-F. Rupprecht, Structure and rheology in vertex models under cell-shape-dependent active stresses, Phys. Rev. Lett. **130**, 058202 (2023).
[41] S. Monfared, G. Ravichandran, J. Andrade, and A. Doostmohammadi, Mechanical basis and topological routes to cell elimination, eLife **12**, e82435 (2023).
[42] R. Sknepnek, I. Djafer-Cherif, M. Chuai, C. J. Weijer, and S. Henkes, Generating active T1 transitions through mechanochemical feedback, eLife **12**, e79862 (2023).
[43] B. I. Halperin and D. R. Nelson, Theory of two-dimensional melting, Phys. Rev. Lett. **41**, 121 (1978).
[44] D. R. Nelson and B. I. Halperin, Dislocation-mediated melting in two dimensions, Phys. Rev. B **19**, 2457 (1979).
[45] Y.-W. Li and M. Pica Ciamarra, Role of cell deformability in the two-dimensional melting of biological tissues, Phys. Rev. Mater. **2**, 045602 (2018).
[46] A. Pasupalak, L. Yan-Wei, R. Ni, and M. Pica Ciamarra, Hexatic phase in a model of active biological tissues, Soft Matter **16**, 3914 (2020).
[47] B. Loewe, M. Chiang, D. Marenduzzo, and M. C. Marchetti, Solid-liquid transition of deformable and overlapping active particles, Phys. Rev. Lett. **125**, 038003 (2020).
[48] C. Zankoc and M. Krajnc, Elasticity, stability, and quasioscillations of cell-cell junctions in solid confluent epithelia, Biophys. J. **119**, 1706 (2020).
[49] M. Krajnc, T. Stern, and C. Zankoc, Active instability and nonlinear dynamics of cell-cell junctions, Phys. Rev. Lett. **127**, 198103 (2021).
[50] J. Rozman, J. M. Yeomans, and R. Sknepnek, Shape-tension coupling produces nematic order in an epithelium vertex model, Phys. Rev. Lett. **131**, 228301 (2023).
[51] https://doi.org/10.5281/zenodo.20393845.
[52] https://doi.org/10.5281/zenodo.20393730.